Atherosclerosis 2014
http://dx.doi.org/10.1016/j.atherosclerosis.2014.09.016

# Osteoglycin deficiency does not affect atherosclerosis in mice

Javier Moncayo-Arlandi [a], Alejandro López-García [b, c], M. Carmen Fernández [b, c], Ana Carmen Durán [b, c], Borja Fernández [b, c, *]

a. *Cardiovascular Genetics Centre, Biomedical Research Institut of Girona, Spain*
b. *Department of Animal Biology, Faculty of Science, University of Ma´laga, Spain*
c. *Biomedical Research Institute of Ma´laga (IBIMA), Spain*

**Abstract**

Objective: The small leucine-rich proteoglycan Osteoglycin/Mimecan (OGN) is a component of the extracellular matrix, where it regulates collagen fibrillogenesis and cytokine availability. OGN is abundant in normal vessels and in atherosclerotic and restenotic lesions of rat, rabbit and human arteries. Osteoglycin-null mice show alterations in the thickness of collagen fibers of the cornea and the skin. In this work, we inspect the possible involvement of OGN in the atherosclerosis progression using a double knockout mouse model. Methods: In order to examine the progression of atherosclerosis in the absence of OGN, we developed double Apoe and Ogn knockout mice and performed a comparative histo-morphological and immunofluorescence study of the atherosclerotic lesions of *Apoe*$^{-/-}$*Ogn*$^{-/-}$ and Apoe$^{-/-}$ *Ogn*$^{+/+}$ mice. Results: We demonstrate the presence of Ogn transcript in the aorta of wildtype mice, its absence in *Ogn*$^{-/-}$ mice, and the normal histomorphology of arteries of *Ogn*$^{-/-}$ mice. The composition of the extracellular matrix and also the cellular content and distribution were similar in atherosclerotic lesions of *Apoe*$^{-/-}$*Ogn*$^{-/-}$ and Apoe$^{-/-}$Ogn$^{+/+}$ mice. Quantification of the lesion size revealed no significant differences between double and single knockout mice. The incidence, size and distribution of calcium deposits were similar in both groups of mice. Conclusions: The lack of the proteoglycan OGN does
not affect the progression of atherosclerosis in mice. Possible causes for the absence of phenotype in the Apoe/Ogn double mutants are discussed.

Keywords: Osteoglycin, Small Leucine-Repeat Domain Protein, Apoe, Knockout mouse.

## Introduction

The structure and composition of the vascular extracellular matrix (ECM) play important regulatory roles in atherogenesis [1]. Some components of the ECM serve as active modulators of the atherosclerotic process. For example, hyaluronic acid modulates

proliferation and inflammation during atherosclerosis and may be pro-atherogenic or anti-atherogenic depending on its polymeric state and amount [2].

The Small Leucine-Repeat Domain Proteins (SLRPs) are localized in the ECM of a variety of tissues, where they regulate matrix homeostasis and modulate cytokine function [3]. The function of SLRPs in matrix homeostasis is driven by their capacity to regulate fibrillogenesis [4], whereas their ability to interact with different members of the transforming grown factor beta (TGF-b) superfamily allow sequestration of cytokine in the matrix [5].

In the vascular system of rats, rabbits and humans, SLRPs are distributed in the various layers of the vessel wall [6e8]. Some of these SLRPs seem to be crucial in maintaining the vascular structural and functional integrity. I. e., absence of Biglycan in mutant mice causes aortic dissection [9], whereas its overexpression increases smooth muscle cell (SMC) proliferation and migration [10]. Some SLRPs have been shown to play a role during atherosclerotic progression. Decorin overexpression in *Apoe* knockout mice causes an increase in collagen content and a reduction of the lesion size [11].

Osteoglycin/Mimecan (OGN) is a proteoglycan belonging to the SLRP family. OGN-deficient ($Ogn^{-/-}$) mice are fertile and show a normal life span. However, they present thicker collagen fibrils in the skin what reduces the tensile strength, but do not show abnormalities of the cornea and cochlea, where OGN is abundant [12e14]. OGN is also present in normal and diseased arteries of rats, rabbits and humans [6e8], but its function and the effect of experimental changes of its expression are unknown.

The aim here is to assess the effect of the absence of OGN in the experimental model of atherosclerosis Apolipoprotein E knockout ($Apoe^{-/-}$) mouse. To address this issue, we have evaluated the progression of atherosclerosis in a double mutant mouse model developed by the intercross between $Apoe^{-/-}$ and $Ogn^{-/-}$ mice.

## Material and methods

### *Animals*

$Apoe^{-/-}$ mice in a C57BL/6 genetic background were obtained from the Jackson Laboratories (Bar Harbor, ME). $Ogn^{-/-}$ mice were developed by Tasheva et al. [12] and backcrossed to C57BL/6 for more than 10 generations. To obtain experimental and control animals ($Apoe^{-/-}Ogn^{-/-}$ and $Apoe^{-/-}Ogn^{+/+}$, respectively), $Apoe^{-/-}$ and $Ogn^{-/-}$ mice were crossed. The resulting heterozygous $F_1$ mice were bred and the appropriate genotypes were selected by PCR analysis of tail DNA.

Animals of 18, 22, 34 and 52 weeks of age were analyzed to cover successive histopathological stages of atherosclerosis progression in $Apoe^{-/-}$ mice [15]. The animals were handled in accordance with the Spanish Regulations for the Protection of Experimental Animals (R.D. 1201/2005; B.O.E. 21.10.2005). All animals were fed regular mouse chow *ad libitum* and sacrificed by carbon dioxide inhalation.

*Ogn transcript detection*

For *Ogn* expression studies, total RNA was extracted from skeletal muscle and aortic arch of both *Apoe*$^{-/-}$*Ogn*$^{-/-}$ and *Apoe*$^{-/-}$*Ogn*$^{+/+}$ mice, with the *mir*Vana™ PARIS™ kit (*Ambion*). To obtain cDNA, the M-MLV RT enzyme (*Invitrogen*) was used. GoTaq Flexi DNA polymerase (*Promega*) was used for PCR. The following primer sequences were used: FW 5'-TTCTCCTGCTACTCTTCGTG-3' and RV 5'-CACACCCATCACAAACATGGG-3'. The PCR products were loaded in a 1.5% agarose gel and the resulting bands were visualized with ethidium bromide.

*Histochemistry and immunofluorescence*

For whole mount histochemistry, the animals were perfusion fixed with 4% paraformaldehyde in phosphate saline buffer (PBS). Then, the aortic arches were dissected out and post-fixed with the same fixative overnight. After several washes with PBS, the speci-mens were stained with 2% Alizarin red S for 10 min, dehydrated with a series of ethanol, cleared up with xilene and preserved in methyl salicilate:benzil benzoate (1:3) solution. The samples were photographed with a Leica MZ10F stereomicroscope equipped with a Leica DFC500 camera.

For histochemistry and immunofluorescence, the cardiac outflow tracts, ascending aorta and aortic arch were fixed overnight with 4% paraformaldehyde in PBS. After dehydration, the speci-mens were embedded in paraffin, and 10 mm thick serial sections were collected on poly-L-Lysine coated slides.

*Histochemical staining*

After deparaffinization, serial sections were stained with Masson-Goldner's trichromic stain for the connective tissue, or alcian blue with the method of Scott and Dorling (0.3 M $MgCl_2$) [16] to identify sulfated glycosaminoglycans, or with the picrosirius-polarization method [17] for the detection of collagen. Microphotographs were obtained using a Leica DMSL microscope with a Leica DFC500 camera.

*Immunofluorescence*

The sections were incubated with Tris-EGTA (pH 9) and microwaved for 15 min. After retrieval, the sections were washed in Tris-PBS (pH 7.8) and incubated first with blocking solution (10% bovine serum, 1% albumin, and 0.5% Triton-X-100 in Tris-PBS) and then with the avidin/biotin blocking kit (*Vector Laboratories*). After the blocking steps, the sections were incubated overnight with a rat anti-CD45 antibody (clone 30 F-11, *BP Pharmigen*) diluted in block solution (1:50) at 4 ◦C. After several washes, the sections were incubated with a goat anti-rat biotin conjugated secondary antibody (*Sigma*) (1:100) for 1 h, washed again, and incubated with FITC conjugated extravidin (1:200) (*Sigma*) for 45 min. After several washes, the sections were incubated with mouse anti-α-SMA-Cy3 antibody (clone 1A4, *Sigma*)

(1:1000) for 1 h and with DAPI (1:1000) for 10 min, washed and mounted with Mowiol (*Sigma*). Microphotographs were obtained with a TSC SP5 confocal microscope (*Leica*).

*Quantification methods*

We used the aortic root of 18 and 22 weeks old Apoe$^{-/-}$*Ogn*$^{+/+}$ and Apoe$^{-/-}$Ogn$^{-/-}$ female and male mice for the morphometric quantification of the lesions size. Two measurements were performed: 1) the relative surface of the lesions (lesion area/vessel area/100) at the central portion of the sinuses of Valsalva of each specimen was estimated using five sections separated by a distance of 30 μm [18]. 2) The surface of the intima and media just beneath the sinotubular level of each specimen were measured, and the intima/media ratio calculated in three sections 20 μm apart [19]. All measurements were performed with the Image J software (NIH).

The appearance of calcification was quantified by calculating the proportion of specimens with calcium deposits in the aortic arch of 22, 34 and 52 weeks old Apoe$^{-/-}$*Ogn*$^{+/+}$ and Apoe$^{-/-}$Ogn$^{-/-}$ male and female mice. The severity of calcified lesions was estimated using a semi-quantification method. We established five degrees of severity (0: without calcification; 1e4: <10%, 10%e25%, 25%e50% and >50% of the aortic arch surface occupied by calcium, respectively). For each stage and sex, the mean degree of severity was obtained.

All graphics and data show the Mean ± SEM. Differences between groups were analyzed using t-Student or $\chi^2$ tests. Differences were considered statistically significant when $p < 0.05$.

**Results**

*Ogn mRNA expression*

To confirm lack of Ogn expression in Ogn mutant mice, we performed a RT-PCR analysis of skeletal muscle and aorta of Apoe$^{-/-}$Ogn$^{-/-}$ (n = 3) and Apoe$^{-/-}$*Ogn*$^{+/+}$ (n = 2) mice (Fig. 1). Ogn mRNA was present in skeletal muscles of Apoe$^{-/-}$*Ogn*$^{+/+}$ mice and absent in Apoe$^{-/-}$Ogn$^{-/-}$ muscles. *Ogn* was also amplified from the aorta of Apoe$^{-/-}$*Ogn*$^{+/+}$ mice, but not from Apoe$^{-/-}$Ogn$^{-/-}$ aortas.

*Atherosclerosis progression*

The Fig. 2A shows the progression of atherosclerotic lesions in the aortic sinuses of 18 (14 males, 14 females), 22 (13 males, 15 females) and 34 (5 males, 7 females) weeks old Apoe$^{-/-}$Ogn$^{-/-}$ and Apoe$^{-/-}$*Ogn*$^{+/+}$ mice. In 18 weeks old mice, some foam cells accumulated in the intima of the aortic sinuses. In 22 and 34 weeks old mice the content of matrix fibers and size of the lesions progressively increased, while dilatation of the sinus walls became evident.
No obvious difference was detected when comparing Apoe$^{-/-}$Ogn$^{-/-}$ and Apoe$^{-/-}$*Ogn*$^{+/+}$ mice.

In order to corroborate our observations, we performed comparative quantifications of the area of the lesions in 18 and 22 weeks old Apoe$^{-/-}$Ogn$^{-/-}$ and Apoe$^{-/-}$*Ogn*$^{+/+}$ mice (Fig.

2B, C). In both stages, the lesions were bigger in females than in males. When the relative surfaces occupied by the lesions were compared (Fig. 2B), the differences between genotypes did not reach statistical significance for any of the genders (18 weeks old: males: 12.73 ± 2.7% vs. 13.35 ± 1.2%, p = 0.858, females: 23.16 ± 4.62% vs. 19.76 ± 2.32%, p = 0.525; 22 weeks old: males: 27.68 ± 6.97% vs. 21.72 ± 4.31%, p = 0.477, females: 34.41 ± 2.41% vs. 37.82 ± 6.57%, p = 0.586). We also calculated the intima/media ratios (Fig. 2C) and again, no significant difference was obtained for any of the genders (18 weeks old: males: 0.185 ± 0.022 vs. 0.122 ± 0.016, p = 0.111, females: 0.309 ± 0.009 vs. 0.298 ± 0.06, p = 0.926; 22 weeks old males: 0.285 ± 0.03 vs. 0.27 ± 0.04, p = 0.793, females: 0.389 ± 0.086 vs. 0.441 ± 0.058, p = 0.67).

*Foam cells and ECM composition of the atherosclerotic lesions*

The Fig. 3A shows the distribution of foam cells and matrix fibers (MT in Fig. 3), sulfated glycosaminoglycans (AB in Fig. 3) and collagen (SR and SRpol in Fig. 3) in lesions of the aortic valve sinuses of 18 weeks old *Apoe*$^{-/-}$*Ogn*$^{+/+}$ (7 males, 7 females) and *Apoe*$^{-/-}$*Ogn*$^{-/-}$ (10 males, 8 females) mice. At this stage, the lesions were mainly formed by groups of foam cells surrounded by few collagen fibers (MT and SR in Fig. 3A). Alcian blue containing 0.3 M $MgCl_2$ stains sulfated glycosaminoglycans, which were abundant in the lesions (AB in Fig. 3A). At this stage, collagen was less abundant than sulfated glycosaminoglycans (SR in Fig. 3A). Under polarized light, Sirius red staining revealed that most collagen fibers in the lesions belonged to the type I collagen (red in SRpol of Fig. 3A).

The composition of sulfated glycosaminoglycans and collagen was similar in lesions of 18 weeks old *Apoe*$^{-/-}$*Ogn*$^{+/+}$ and *Apoe*$^{-/-}$*Ogn*$^{-/-}$ mice. Likewise, the amount of these molecules and foam cells did not seem to vary between these two groups of mice.

The Fig. 3B shows the distribution of foam cells, sulfated glycosaminoglycans and collagen in lesions of the aortic valve sinuses of 22 weeks old *Apoe*$^{-/-}$*Ogn*$^{+/+}$ (7 males, 7 females) and *Apoe*$^{-/-}$*Ogn*$^{-/-}$ (10 males, 8 females) mice. The sulfated glycosaminoglycans were more abundant than in lesions of 18 weeks old mice and accumulated in the inner surface of the lesions (AB in Fig. 3B). Collagen was also more abundant than in the previous stage, forming the fibrous caps (SR in Fig. 3B). At this stage, the presence of collagen type III was also patent (green and yellow in SRpol of Fig. 3B).

As in the previous stage, the composition and amount of foam cells and ECM components was similar in *Apoe*$^{-/-}$*Ogn*$^{+/+}$ and *Apoe*$^{-/-}$*Ogn*$^{-/-}$ mice.

*Cellular composition of the atherosclerotic lesions*

$CD45^+$ leukocytes, most of them in form of foam cells, were abundant in the lesions of 18 weeks old mice (CD45 in Fig. 4A). In 22 weeks old mice, the proportion of $CD45^+$ cells decreased. A stronger signal was detected in the subendothelial layer (open arrows in Fig. 4B). The amount and distribution of $CD45^+$ leukocytes in the lesions of 18 and 22 weeks old mice

was similar when *Apoe*$^{-/-}$*Ogn*$^{+/+}$ (5 males, 5 females) and *Apoe*$^{-/-}$*Ogn*$^{-/-}$ (5 males, 5 females) specimens were compared.

In 18 weeks old mice, a-SMA$^{+}$ cells were detected in the aortic sinus walls and in the edge of the lesions (arrowheads in Fig. 4A). In 22 weeks old mice, a significantly higher number of SMCs populated the lesions. The distribution of these cells paralleled that of collagen fibers, surrounding the fibrous cap (SR in Fig. 3B and arrowheads in Fig. 4B). No evident differences were detected in the amount and distribution of SMCs of the lesions when *Apoe*$^{-/-}$*Ogn*$^{+/+}$ (5 males, 5 females) and *Apoe*$^{-/-}$*Ogn*$^{-/-}$ (5 males, 5 females) specimens were compared.

*Calcification*

Calcium deposits were first observed at the lesser curvature of the aortic arch and at areas of branching of the aortic arch arteries in 22 weeks old mice. In 34 weeks old mice, more and bigger deposits were detected at the same positions. In 52 weeks old mice, the calcium deposits formed long plaques, covering the lesser curvature of the aortic arch and the stem of the aortic arch arteries (Fig. 5A; the number of specimens analyzed are detailed in the graphs of Fig. 5B, C).

The presence and localization of the calcium deposits were similar in *Apoe*$^{-/-}$*Ogn*$^{+/+}$ and *Apoe*$^{-/-}$*Ogn*$^{-/-}$ mice. However, in both groups the aortic arches of females contained more and bigger calcium deposits than those of males with the same age. The Fig. 5B shows the proportion of animals with calcium deposits for each sex and stage analyzed. In both sexes, single or double mutants, calcification progressed from 22 weeks of age onward. Calcium deposits were present in most 34 weeks old females, whereas only half of males showed calcium deposits at this stage. No significant statistical differences were obtained when comparing *Apoe*$^{-/-}$*Ogn*$^{+/+}$ with *Apoe*$^{-/-}$*Ogn*$^{-/-}$ males or females at each stage.

The analysis of the severity of calcification showed a progressive increase of the aortic surface occupied by calcium with age (Fig. 5C). We observed a low degree of calcification in 22 weeks old *Apoe*$^{-/-}$*Ogn*$^{+/+}$ and *Apoe*$^{-/-}$*Ogn*$^{-/-}$ mice, without significant differences between genotypes (males: 0.28 ± 0.2 *vs.* 0.114 ± 0.085, $p = 0.097$; and females: 0.2 ± 0.089 *vs.* 0.285 ± 0.129, $p = 0.63$). In 34 weeks old mice, the severity of calcification increased, but in a similar proportion in both genotypes (males: 0.816 ± 0.164 *vs.* 0.816 ± 0.246, $p = 1$; females: 1.366 ± 0.13 *vs.* 1.357 ± 0.266, $p = 0.976$). In 52 weeks old mice, a further increase in severity without differences between genotypes was noted (males: 1.577 ± 0.395 *vs.* 2.5 ± 0.264, $p = 0.098$, females: 1.946 ± 0.175 *vs.* 2.75 ± 0.419, $p = 0.096$).

*Discussion*

The different members of the SLRP family of proteoglycans have common roles in regulating vascular matrix homeostasis and tissue remodeling [6,9,20e22]. They play this regulatory role by acting on collagen fibrillogenesis, cytokine availability in the matrix and SMCs proliferation [3]. These functions of SLRPs in the vascular system anticipate their

involvement in the development of vascular diseases. In fact, several SLRPs have been shown to coexist in atherosclerotic lesions [8,23] and their overexpression have profound effects on disease progression [10,11,24].

Like the other SLRPs, the main function of OGN in the ECM is to regulate collagen type I fibrillogenesis [12,25]. OGN deficient mice show reduced thickness of collagen fibers in the skin, causing a decrease of the tensile strength [12]. Another function of OGN is to regulate vascular SMC proliferation. In both humans and animal models, OGN downregulation is required for SMC proliferation both in vitro and in vivo [6,7,26]. In addition, OGN was initially named Osteoinductive Factor (OIF) after it was isolated from bovine bone extracts, bound to TGF-b1 and -2 [27], accordant with a role in bone formation [28]. Thus, OGN is involved in three biological processes, which are crucial for atherosclerosis progression: collagen fibrillogenesis, SMC proliferation and calcification.

OGN expression and localization are highly regulated during atherosclerotic progression in human and animal models [6,7]. In order to inspect its involvement in the atherosclerotic process, we analyzed the disease progression in *Apoe*$^{-/-}$*Ogn*$^{-/-}$ double knockout mice compared to that of *Apoe*$^{-/-}$ knockout mice. Given that OGN is involved in molecular and cellular mechanisms that are crucial for atherosclerosis to proceed, namely collagen fibrillogenesis, SMC proliferation and calcification, we focused on the size of the lesions, the composition of the ECM, the distribution of SMCs and the calcification of the plaques.

To validate our experimental design and animal model we assessed the expression of *Ogn* in the aorta of wildtype and *Apoe*$^{-/-}$ knockout mice by RT-PCR, and its absence in *Ogn*$^{-/-}$ and *Apoe*$^{-/-}$*Ogn*$^{-/-}$ mutants (Fig. 1). As previously described, *Ogn*$^{-/-}$ mutantmice were fertile and showed a normal life span [12]. Likewise, the fertility, life spam and wellness of *Apoe*$^{-/-}$*Ogn—/—* mice were comparable to those of *Apoe*$^{-/-}$ mutants. Despite the known function of OGN in fibrillogenesis and its presence in the ECM of the normal aorta, the general anatomy and histology of the cardiovascular system of *Ogn*$^{-/-}$ knockout mice (heart, thoracic arteries, abdominal artery, portal and renal arteries, and limb vasculature) were normal and similar to that of wildtype mice (data not shown). In addition, the type, amount and distribution of collagen were not altered in the atherosclerotic lesions of double mutant mice compared to *Apoe*$^{-/-}$ mutants (Fig. 3). It is known that OGN is abundant in the skin, which also shows a normal anatomy and histology in *Ogn* knockout mice [12]. However, an ultrastructural study of collagen fibers in the skin of these mice revealed alterations in their thickness, resulting in a reduction of the tensile strength of the tissue [12]. Although ultrastructural alterations of collagen fibers might be also present in atherosclerotic lesions of *Apoe*$^{-/-}$*Ogn*$^{-/-}$ mice, these did not affect lesion size or content. Likewise, the stability of the plaques did not seem to be compromised in *Apoe*$^{-/-}$*Ogn*$^{-/-}$ mice, as aged double mutants did not show higher mortality than *Ogn*$^{-/-}$ mice.

The composition and distribution of both the cellular and ECM components of the atherosclerotic lesions varied similarly in 18, 22 and 34 weeks old *Apoe*$^{-/-}$*Ogn*$^{+/+}$ and *Apoe*$^{-}$

$^{/-}$*Ogn*$^{-/-}$ mice (Figs. 2A and 3). Furthermore, comparative quantifications of the area of the lesions and of the intima/media ratio in 18 and 22 weeks old mice revealed no significant differences between genotypes (Fig. 2B, C). Hence, early lesion progression and severity were not affected by OGN deficiency.

OGN may be linked to glycosaminoglycans like keratan-sulfate in different tissues [12,29], though it also may present without sugar chains in aorta [7,29]. In both *Apoe*$^{-/-}$*Ogn*$^{+/+}$ and *Apoe*$^{-/-}$*Ogn*$^{-/-}$ mutants, the amount and distribution of sulfated glycosaminoglycans did not differ between lesions of single and double mutants (Fig. 3). Previous studies in Watanabe rabbits showed that OGN proteoglycan is abundant in the neointima of atherosclerotic lesions [7]. The fact that OGN deficiency does not alter the proteoglycan content of mouse atherosclerotic lesions can be interpreted as the result of compensation by other SLRP proteoglycans. In fact, this type of compensatory mechanism has been observed in knockout mouse models for different SLRPs [30,31].

OGN has been shown to negatively regulate proliferation of SMCs both *in vitro* and *in vivo* [6,21,26]. We then predicted that absence of OGN in the aortic matrix would lead to an increase in the SMC content of the atherosclerotic lesions. In *Apoe*$^{-/-}$*Ogn*$^{+/+}$ and *Apoe*$^{-/-}$ *Ogn*$^{-/-}$ specimens we observed that the amount of leukocytes decreased whereas that of SMCs increased with age. SMCs first appeared in the subendothelium, to finally surround the fibrous cap (Fig. 4). However, no evident differences were detected in the amount and distribution of leucocytes and SMCs when *Apoe*$^{-/-}$*Ogn*$^{+/+}$ and *Ogn*$^{-/-}$*Apoe*$^{-/-}$ specimens were compared. Moreover, quantification of the lesions size revealed no significant difference between single and double mutants (Fig. 2B, C).

Calcification of the late atherosclerotic lesion is mediated by osteogenic growth factors of the TGF-b superfamily [32]. Some SLRPs, including OGN, are able to interact with distinct TGF-b members [5,33]. *In vitro*, OGN is able to induce osteogenic fate and mineralization mediated by TGF-b signaling [34]. In addition, some SLRPs like Decorin have been found associated with calcification cores in human atherosclerotic plaques [35]. Consequently, we hypothesized that OGN deficiency would alter the calcification progression in *Apoe*$^{-/-}$*Ogn*$^{-/-}$ mice. We detected that calcium deposits were present in atherosclerotic lesions of 22e52 weeks old mice (Fig. 5). The calcium deposits grew earlier and faster in females than in males, as previously described for *Apoe*$^{-/-}$ mutant mice [36]. However, quantification of the occurrence of calcium deposits (Fig. 5B), as well as severity of calcification (Fig. 5C) in *Apoe*$^{-}$ $^{/-}$*Ogn*$^{+/+}$ and *Apoe*$^{-/-}$*Ogn*$^{-/-}$ animals revealed no significant difference between males or females. Likewise, the size and localization of the deposits seemed not to vary between both types of mutants (Fig. 5A).

In summary, our results show that compared to *Apoe* knockout mice, *Apoe-Ogn* double knockouts have normal life span and wellness, atherosclerotic lesions of similar size with normal composition of the matrix and cellular components, as well as normal progression and

severity of lesion calcification. Taken together, our results indicate that absence of OGN do not alter atherosclerosis progression in mice.

Previous studies already showed that some of the organs where OGN is abundant, like cornea and cochlea [29], develop normally in *Ogn* knockout mice [13,14]. However, in other tissues, absence of OGN causes functional alterations like reduced tensile strength of the skin [12]. In cardiac tissue, permissive physiological perturbation is required to reveal a phenotype in *Ogn* knockout mice, as prohypertrophic stimulation with angiotensin II infusion induces a significant attenuation in the left ventricular mass response compared to wildtype mice [37]. We show here that OGN deficiency has no effect on both normal arterial development and pathological atherosclerotic progression. It can be concluded that OGN is dispensable in particular homeostatic and pathogenic process of some tissues, including the vascular system. Compensation of OGN deficiency by similar glycoproteins of the SLRP family may explain this effect. Indeed, this compensatory mechanism has been described in tendon and cornea of Fibromodulin and Decorin deficient mouse models respectively [30,31]. Nonetheless, the expression of different SLRP genes is regulated by common transcription factors [33], what may offer a plausible molecular mechanism for this hypothetical compensatory effect to take place. Biglycan and Decorin are good candidates for compensating OGN deficiency in atherosclerotic lesions, as these SLRP proteoglycans are enriched in the atherosclerotic lesion as it increases in size and complexity [23]. Additional experiments of SLRP mRNA and protein quantification in atherosclerotic aortas of *Apoe-Ogn* double knockout mice are needed to test the compensation hypothesis.


## Acknowledgments

*Ogn*$^{-/-}$ mice were produced by Eli Lilly, Inc., and made available to the authors. The authors thank David Navas, Málaga, for his assistance with the confocal microscope.

## Sources of funding

This work was supported by Grants SAF2006-01548 from Min- isterio de Educacio´n y Ciencia (Madrid, Spain); P10-CTS-06068 from Junta de Andalucía (Sevilla, Spain); and Red de Investigacio´n Cardiovascular (RIC; RETICs) (Madrid, Spain)


## References


[1] Orr AW, Hastings NE, Blackman BR, et al. Complex regulation and function of the inflammatory smooth muscle cell phenotype in atherosclerosis. J. Vasc. Res. 2010;47:168e80.

[2] Bot PT, Hoefer IE, Piek JJ, et al. Hyaluronic acid: targeting immune modulatory components of the extracellular matrix in atherosclerosis. Curr. Med. Chem. 2008;15:786e91.

[3] Merline R, Schaefer RM, Schaefer L. The matricellular functions of small leucine-rich proteoglycans (SLRPs). J. Cell Commun. Signal. 2009;3:323e35.

[4] Kalamajski S, Oldberg A. The role of small leucine-rich proteoglycans in collagen fibrillogenesis. Matrix Biol. J. Int. Soc. Matrix Biol. 2010;29:248e53.

[5] Hildebrand A, Romaris M, Rasmussen LM, et al. Interaction of the small interstitial proteoglycans biglycan, decorin and fibromodulin with transforming growth factor beta. Biochem. J. 1994;302(Pt 2):527e34.

[6] Shanahan CM, Cary NR, Osbourn JK, et al. Identification of osteoglycin as a component of the vascular matrix. Differential expression by vascular smooth muscle cells during neointima formation and in atherosclerotic plaques. Arterioscler. Thromb. Vasc. Biol. 1997;17:2437e47.

[7] Fernandez B, Kampmann A, Pipp F, et al. Osteoglycin expression and localization in rabbit tissues and atherosclerotic plaques. Mol. Cell. Biochem. 2003;246:3e11.

[8] Strom A, Ahlqvist E, Franzen A, et al. Extracellular matrix components in atherosclerotic arteries of Apo E/LDL receptor deficient mice: an immuno- histochemical study. Histol. Histopathol. 2004;19:337e47.

[9] Heegaard AM, Corsi A, Danielsen CC, et al. Biglycan deficiency causes spontaneous aortic dissection and rupture in mice. Circulation 2007;115:2731e8.

[10] Shimizu-Hirota R, Sasamura H, Kuroda M, et al. Extracellular matrix glycoprotein biglycan enhances vascular smooth muscle cell proliferation and migration. Circ. Res. 2004;94:1067e74.

[11] Al Haj Zen A, Caligiuri G, Sainz J, et al. Decorin overexpression reduces atherosclerosis development in apolipoprotein E-deficient mice. Atherosclerosis 2006;187:31e9.

[12] Tasheva ES, Koester A, Paulsen AQ, et al. Mimecan/osteoglycin-deficient mice have collagen fibril abnormalities. Mol. Vis. 2002;8:407e15.

[13] Beecher N, Carlson C, Allen BR, et al. An x-ray diffraction study of corneal structure in mimecan-deficient mice. Investig. Ophthalmol. Vis. Sci. 2005;46: 4046e9.

[14] Williamson RE, Darrow KN, Giersch AB, et al. Expression studies of osteoglycin/mimecan (OGN) in the cochlea and auditory phenotype of Ogn-deficient mice. Hear. Res. 2008;237:57e65.

[15] Reddick RL, Zhang SH, Maeda N. Atherosclerosis in mice lacking apo E. Evaluation of lesional development and progression. Arterioscler. Thromb. J. Vasc. Biol./Am. Heart Assoc. 1994;14:141e7.

[16] Scott JE, Dorling J. Differential staining of acid glycosaminoglycans (mucopolysaccharides) by alcian blue in salt solutions. Histochimie 1965;5:221e33.

[17] Junqueira LCV, Bignolas G, Brentani RR. Picrosirius staining plus polarization microscopy, a specific method for collagen detection in tissue sections. Histochem. J. 1979;11:435e47.

[18] Paigen B, Morrow A, Holmes PA, et al. Quantitative assessment of atherosclerotic lesions in mice. Atherosclerosis 1987;68:231e40.

[19] Shami A, Gustafsson R, Kalamajski S, et al. Fibromodulin deficiency reduces low-density lipoprotein accumulation in atherosclerosis plaque in apolipoprotein E-null mice. Arterioscler. Thromb. Vasc. Biol. 2012;33:354e61.

[20] Jian J, Zheng Z, Zhang K, et al. Fibromodulin promoted in vitro and in vivo angiogenesis. Biochem. Biophys. Res. Commun. 2013;436:530e5.

[21] Kampmann A, Fernandez B, Deindl E, et al. The proteoglycan osteoglycin/mimecan is correlated with arteriogenesis. Mol. Cell. Biochem. 2009;322: 15e23.

[22] Scott RA, Paderi JE, Sturek M, et al. Decorin mimic inhibits vascular smooth muscle proliferation and migration. PloS One 2013;8:e82456.

[23] Marzoll A, Melchior-Becker A, Cipollone F, et al. Small leucine-rich proteoglycans in atherosclerotic lesions: novel targets of chronic statin treat- ment? J. Cell. Mol. Med. 2011;15:232e43.

[24] Fischer JW, Kinsella MG, Clowes MM, et al. Local expression of bovine decorin by cell-mediated gene transfer reduces neointimal formation after balloon injury in rats. Circ. Res. 2000;86:676e83.

[25] Ge G, Seo NS, Liang X, et al. Bone morphogenetic protein-1/tolloid-related metalloproteinases process osteoglycin and enhance its ability to regulate collagen fibrillogenesis. J. Biol. Chem. 2004;279:41626e33.

[26] Gu XS, Lei JP, Shi JB, et al. Mimecan is involved in aortic hypertrophy induced by sinoaortic denervation in rats. Mol. Cell. Biochem. 2011;352:309e16.

[27] Bentz H, Nathan RM, Rosen DM, et al. Purification and characterization of a unique osteoinductive factor from bovine bone. J. Biol. Chem. 1989;264: 20805e10.

[28] Hamajima S, Hiratsuka K, Kiyama-Kishikawa M, et al. Effect of low-level laser irradiation on osteoglycin gene expression in osteoblasts. Lasers Med. Sci. 2003;18:78e82.

[29] Funderburgh JL, Corpuz LM, Roth MR, et al. Mimecan, the 25-kDa corneal keratan sulfate proteoglycan, is a product of the gene producing osteoglycin. J. Biol. Chem. 1997;272:28089e95.

[30] Svensson L, Aszodi A, Reinholt FP, et al. Fibromodulin-null mice have abnormal collagen fibrils, tissue organization, and altered lumican deposition in tendon. J. Biol. Chem. 1999;274:9636e47.

[31] Zhang G, Chen S, Goldoni S, et al. Genetic evidence for the coordinated regulation of collagen fibrillogenesis in the cornea by decorin and biglycan. J. Biol. Chem. 2009;284:8888e97.

[32] Johnson RC, Leopold JA, Loscalzo J. Vascular calcification: pathobiological mechanisms and clinical implications. Circ. Res. 2006;99:1044e59.

[33] Tasheva ES, Klocke B, Conrad GW. Analysis of transcriptional regulation of the small leucine rich proteoglycans. Mol. Vis. 2004;10:758e72.

[34] Tanaka K, Matsumoto E, Higashimaki Y, et al. Role of osteoglycin in the linkage between muscle and bone. J. Biol. Chem. 2012;287:11616e28.

[35] Fischer JW, Steitz SA, Johnson PY, et al. Decorin promotes aortic smooth muscle cell calcification and colocalizes to calcified regions in human atherosclerotic lesions. Arterioscler. Thromb. Vasc. Biol. 2004;24:2391e6.

[36] Bennett BJ, Scatena M, Kirk EA, et al. Osteoprotegerin inactivation accelerates advanced atherosclerotic lesion progression and calcification in older ApoE$^{-/-}$ mice. Arterioscler. Thromb. Vasc. Biol. 2006;26:2117e24.

[37] Petretto E, Sarwar R, Grieve I, et al. Integrated genomic approaches implicate osteoglycin (Ogn) in the regulation of left ventricular mass. Nat. Genet. 2008;40:546e52.

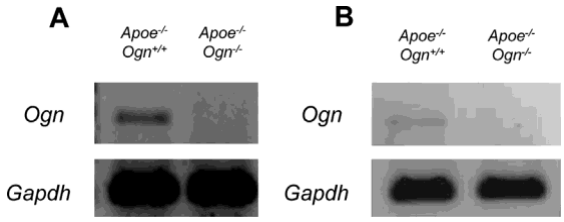


Fig. 1. RT-PCR analysis of Ogn expression in *Apoe*$^{-/-}$*Ogn*$^{-/-}$ and *Apoe*$^{-/-}$*Ogn*$^{+/+}$ mice. A) Note a clear band corresponding to Ogn transcript from skeletal muscle of *Apoe*$^{-/-}$*Ogn*$^{+/+}$ mice, and absence of the band in double knockout (*Apoe*$^{-/-}$*Ogn*$^{-/-}$). B) In the aortic arch, a faint but detectable band is observed in *Apoe*$^{-/-}$*Ogn*$^{+/+}$ mice, which is absent in double knockouts.

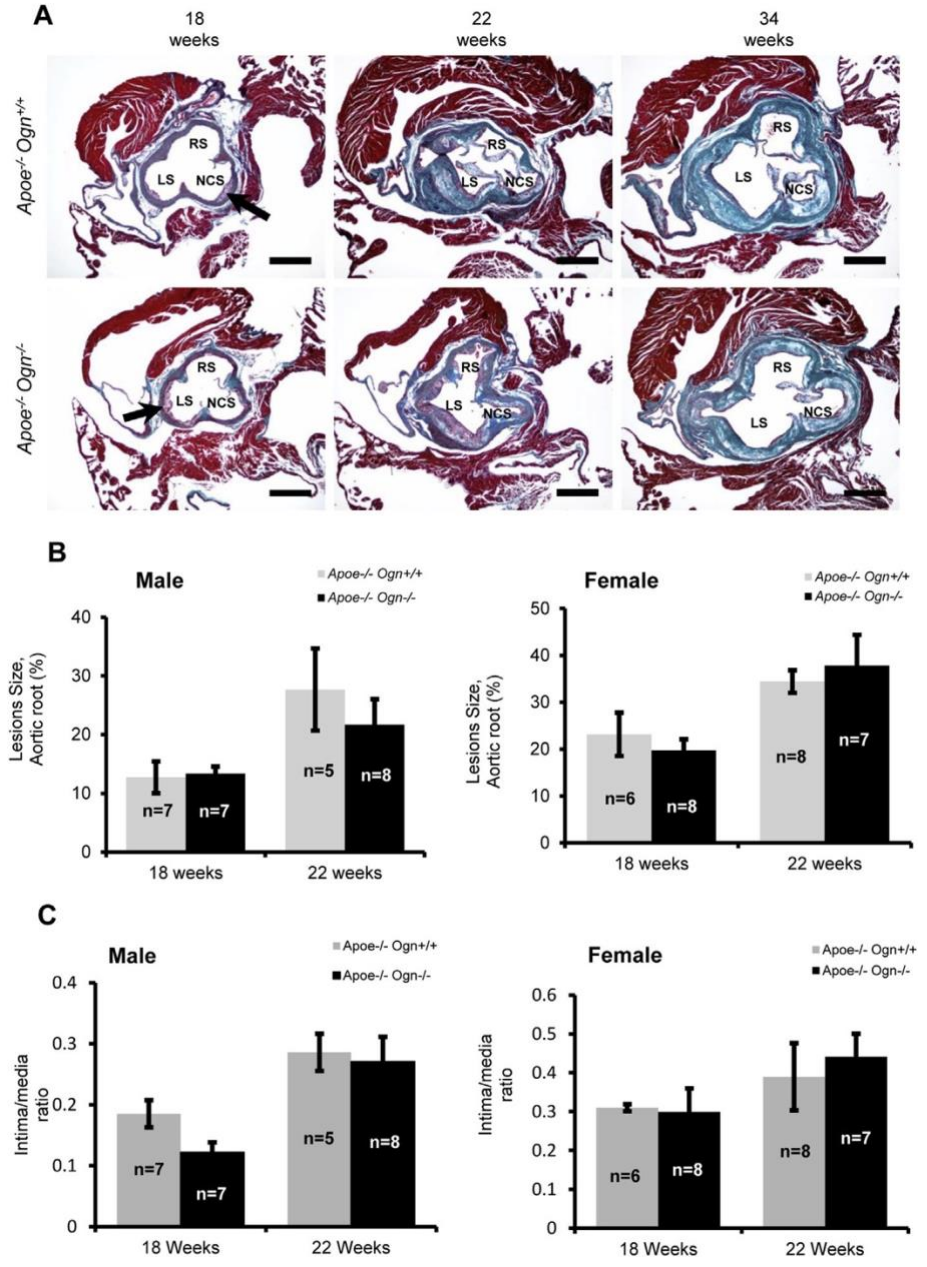


Fig. 2. Atherosclerosis progression in *Apoe*$^{-/-}$*Ogn*$^{-/-}$ and *Apoe*$^{-/-}$*Ogn*$^{+/+}$ mice. A) Masson-Goldner's trichromic staining of the aortic root of 18, 22 and 34 weeks old *Apoe*$^{-/-}$*Ogn*$^{+/+}$ and *Apoe*$^{-/-}$*Ogn*$^{-/-}$ mice. Foam cells are stained brown in lesions of 18 weeks old mice (arrows). At later stages, the lesions become progressively richer in matrix fibers (green). B,C) The relative size of the lesions was compared between *Apoe*$^{-/-}$*Ogn*$^{+/+}$ and *Apoe*$^{-/-}$*Ogn*$^{-/-}$ male and female mice of 18 and 22 weeks of age, expressed as the relative lesion surface (B) and the intima/media ratio (C). *n* = number of animals analyzed per group; NCS = noncoronary sinus; LS = left sinus; RS = right sinus. Bars = 500 μm. (For interpretation of the references to color in this figure legend, the reader is referred to the web version of this article.)

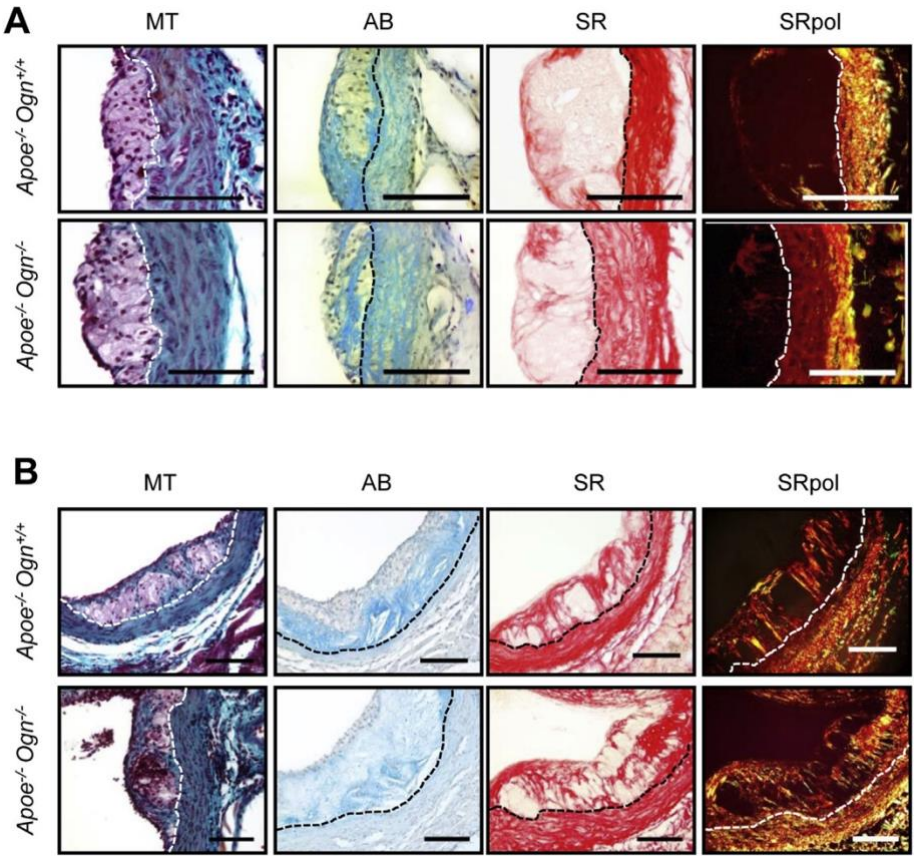


Fig. 3. Foam cells and ECM composition of the atherosclerotic lesions in *Apoe*$^{-/-}$*Ogn*$^{-/-}$ and *Apoe*$^{-/-}$*Ogn*$^{+/+}$ mice. Masson-Goldner's trichromic (MT), alcian blue (AB; 0.3 M $MgCl_2$), Sirius red (SR), and Sirius red under polarized light (SRpol) stainings of atherosclerotic lesions of 18 (A) and 22 (B) weeks old *Apoe*$^{-/-}$*Ogn*$^{+/+}$ and *Apoe*$^{-/-}$*Ogn*$^{-/-}$ mice. The discontinuous line marks the internal elastic lamina. At least forty sections per specimen were analyzed. More explanations in the text. Bars = 100 μm. (For interpretation of the references to color in this figure legend, the reader is referred to the web version of this article.)

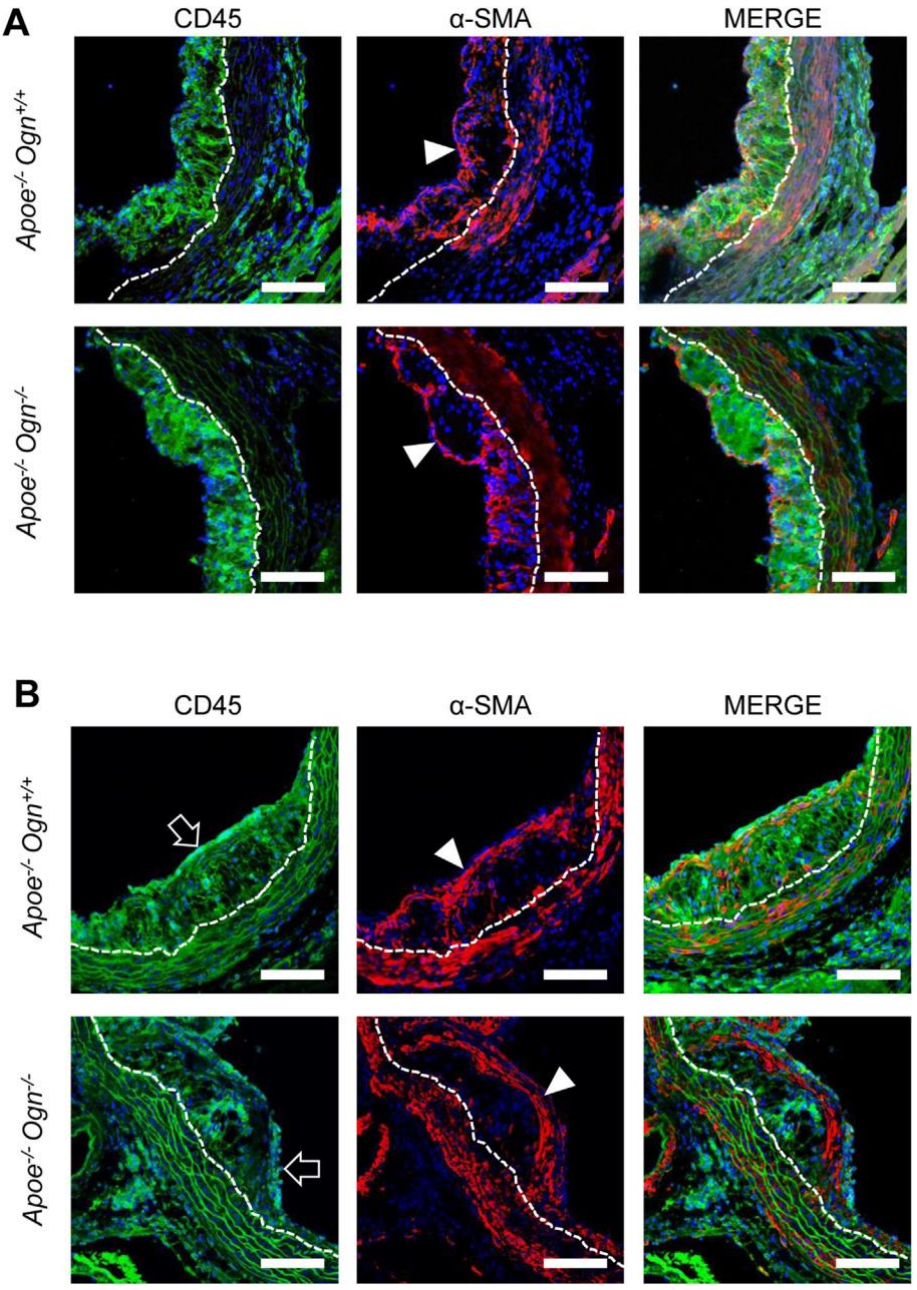


Fig. 4. Cellular composition of the atherosclerotic lesions in *Apoe*$^{-/-}$*Ogn*$^{-/-}$ and *Apoe*$^{-/-}$*Ogn*$^{+/+}$ mice. Confocal triple immunofluorescence of four representative sections of atherosclerotic lesions from 18 (A) and 22 (B) weeks old *Apoe*$^{-/-}$*Ogn*$^{-/-}$ and *Apoe*$^{-/-}$*Ogn*$^{+/+}$ mice. The autofluorescence of the elastic lamina was evident in some sections of the aortic root wall. The discontinuous line marks the internal elastic lamina. At least ten sections per specimen were analyzed. Blue: nuclear staining (DAPI); green: CD45; red: a-SMA. More explanations in the text. Bars = 50 μm. (For interpretation of the references to color in this figure legend, the reader is referred to the web version of this article.)

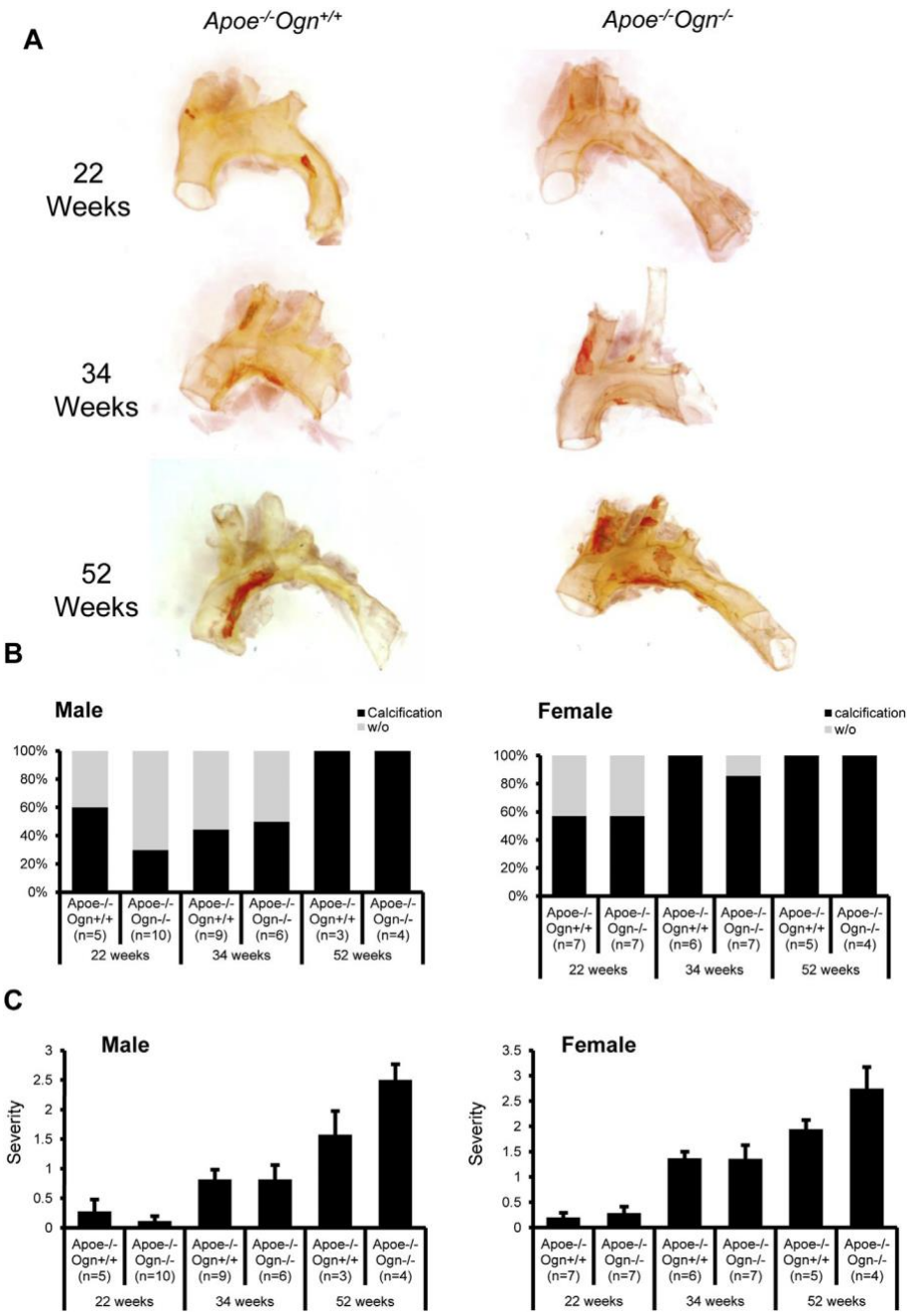


Fig. 5. Calcification in lesions of *Apoe*$^{-/-}$*Ogn*$^{-/-}$ and *Apoe*$^{-/-}$*Ogn*$^{+/+}$ mice. A) Representative microphotographs of the aortic arches of 22, 34 and 52 weeks old *Apoe*$^{-/-}$*Ogn*$^{-/-}$ and *Apoe*$^{-/-}$*Ogn*$^{+/+}$ mice stained with alizarin red. B) Incidence of calcium deposits in male and female *Apoe*$^{-/-}$*Ogn*$^{+/+}$ and *Apoe*$^{-/-}$*Ogn*$^{-/-}$ mice. Data are shown as percentage of aortic arch with (black) and without (gray) calcium deposits. C) Severity of calcification expressed as relative surface of the artery occupied by calcium deposits. *n* = number of animals analyzed. (For interpretation of the references to color in this figure legend, the reader is referred to the web version of this article.)